Electron spectroscopy in proton collisions with dry gas-phase uracil base

Patrick Moretto-Capelle and Arnaud Le Padellec
Laboratoire Collisions, Agrégats, Réactivité (UMR 5589 CNRS-UPS), IRSAMC, Université Paul Sabatier Toulouse 3, 31062 Toulouse Cedex 9, France

(Received 10 February 2006; revised manuscript received 6 October 2006; published 8 December 2006)

We have investigated the electron emission by the RNA uracil base ($C_4H_4N_2O_2$) due to collisions with protons in the 25 keV–100 keV energy range. Electron spectroscopy was performed at 35° with respect to the beam direction and absolute values for the double-differential cross section were obtained. Our results show preferential emission of low-energy electrons that are responsible for damage in biological material through dissociative electron attachment [Boudaïffa *et al.*, Science **287**, 1658 (2000)]. Experimental results are compared to calculations that used the classical trajectory Monte Carlo method, and a reasonable agreement is obtained.

DOI: 10.1103/PhysRevA.74.062705 PACS number(s): 34.50.Gb

INTRODUCTION

The effects of radiation on biological systems can be related to alteration of DNA by single and/or double strand breaks that might lead to a cell's death or might generate mutation. For a long time, there was a gap in our understanding in between (macroscopic) biological effects and (microscopic) molecular interaction of ionizing radiation on the "building blocks of life" such as the DNA or RNA bases. However, some years ago it was acknowledged that biological effects, such as a cell's death or DNA strand breaks, can be directly linked to "pure" atomic physic mechanisms like inner shell ionization followed by the Auger effect [1,2], or more recently, to molecular ones through the effect of low-energy electrons via the electron dissociative attachment mechanism [3–5]. Ionizing radiation (X, e^-, heavy ions) is now commonly used in cancer therapy to irradiate "risk zones" or tumors. In particular, with proton therapy, the energy is deposited along the depth in a well-defined zone (Bragg peak). The particle is slowly decelerated in the biological medium until it reaches the energy at which the linear energy transfer (LET), or stopping power, is maximal (around 100 keV). The localization of the dose deposit is a considerable advantage that enables brain and eye tumors to be treated. At those high energies, the slowing down of ions in the bulk is mainly due to ionization, and a manifold of secondary electrons is also created [6,7]. Those electrons will further interact with the surrounding molecules and give rise to damage that are kinetic energy specific, that is, fragmentation and ionization of DNA constituents by high-energy electrons ($>$20 eV), and dissociative attachment by low-energy electrons ($<$10 eV) with direct or indirect damages via the dissociation of water molecules. Therefore, the complete characterization of the electronic emission (kinetic energy and angular distribution) is of great importance, and the corresponding double-differential cross section can be used as input data in track's calculations [7–9] as well as in electronic thermalization issues [10,11].

In this paper, we present the first electron spectrum resulting from collisions between protons and gas-phase uracil. The collision energy range extends from 25 keV to 100 keV, the latter corresponding to the maximum of LET in biological media. Absolute values for the double-differential cross sections (DDCS) are obtained for an angle of 35° with respect to the beam direction. Future experiments are planned to include the angular distribution in the emission, with the goal that this might be useful in track's calculations. Results are discussed and put in perspective with those from a classical trajectory Monte-Carlo (CTMC) calculation.

EXPERIMENTAL

A 25, 50, and 100 keV proton ion beam impinged on a jet of uracil that was produced by an oven heated to about 120 °C that was loaded with a commercial powder. Electrons were energy analyzed by means of an electrostatic cylindrical mirror analyzer (CMA) whose energy resolution is 1% [12]. The CMA device selected electrons that were emitted at 35° with respect to the ion beam incident direction. Electrons were detected and counted on a channeltron. Spurious electron emission in the absence of any molecular target was systematically subtracted in every spectrum and a correction was applied to the electron transmission efficiency (comparison of an electron spectrum obtained for a 100-keV proton beam versus an He target to tabulated data by Rudd *et al.* [13]).

To determine the absolute DDCS, we had to account simultaneously for the unknown target density and its fluctuation. We therefore had to record both the electron yield at a given energy E_e and something that reflects another known collisional process. We chose to monitor the yield of protons that were elastically scattered at right angles, according to a protocol previously used in nuclear physics [14]. We had to record simultaneously both the electrons that traveled through the CMA at a given energy, we chose an energy value of 50 eV as a compromise between the counting rate and spurious noise, and elastic scattering projectiles.

The number of detected electrons N_e is given by

$$N_e = \frac{\partial^2 \sigma_e}{\partial \Omega_e \partial E_{e(35°,50\ \mathrm{eV})}} \quad [nl\Delta\Omega]_e \Delta E_e \eta_e N_{proj}, \qquad (1)$$

where $\partial^2\sigma_e/\partial\Omega_e\partial E_{e(35°,50\ \mathrm{eV})}$ depicts the DDCS for the production of secondary electrons to be normalized for the fixed

angle of 35° and electron energy E_e of 50 eV, respectively. The parameters $[nl\Delta\Omega]_e$ represent the target density profile, interaction length, and solid angle seen by the CMA, respectively. Note that the jet profile had to be evaluated independently via a thickness measurement of a uracil deposit on a glass surface. ΔE_e depicts the energy bandwidth of the CMA. Electrons were accelerated through a 300 V potential difference prior to any detection on the Channeltron. The resulting electron detection efficiency was $\eta_e=0.9$ [15]. Last, the number of projectiles is N_{proj}.

The number of ions N_i, elastically scattered at right angles, is

$$N_i = \frac{\partial\sigma_i}{\partial\Omega_{i_{ES}}}[nl\Delta\Omega]_i \eta_i N_{proj}, \tag{2}$$

where $\partial\sigma_i/\partial\Omega_{i_{ES}}$ represents the single differential cross sections for elastic scattering at 90°. The parameters $[nl\Delta\Omega]_\iota$ represent the target density profile, interaction length, and solid angle seen by the detector that records the scattered ions, i.e., a multichannel plate (MCP) assembly, respectively. As a matter of fact, the detection efficiency η_i for ions by a microchannel plate is a nontrivial issue. Gao *et al.* [16] have shown that the ion recording efficiency reaches a maximum for proton energies $E>5$ keV. In our case, protons were scattered with larger energies, that is to say, 7.16 keV. Gao *et al.* measured a maximum in efficiency of about 60% for an open area ratio (OAR) of the MCP, and also made the important finding that a low negative potential set in front of the first MCP repels very efficiently the secondary electrons emitted by the surface. This substantially increases the detection efficiency, an effect observed by Funsten *et al.* [17], who reported an efficiency of 87%. This is also confirmed by Martin *et al.* [18] with a value of about 85%. Moreover, an exhaustive study of the influence of a negatively biased grid placed in front of the first plate was carried out by Deconihout *et al.* [19], who found a value of ~90% for the MCP detection efficiency. We also performed a direct measurement of the absolute efficiency by means of a correlation technique in the CO_2^{2+} dissociation, and we obtained a value of 95±5%.

The absolute DDCS for electron emission are obtained by combining Eqs. (1) and (2),

$$\frac{\partial^2\sigma_e}{\partial\Omega_e\partial E_e} = \frac{N_e}{N_i}\frac{\partial\sigma_i}{\partial\Omega_i}\frac{[nl\Delta\Omega]_i}{[nl\Delta\Omega]_e}\frac{1}{\Delta E_e}\frac{\eta_i}{\eta_e}. \tag{3}$$

It is worth noticing that the DDCS absolute values are directly linked to the ionic detection efficiency and that an overestimation of this parameter will subsequently lead to an overestimation of the cross sections.

The $[nl\Delta\Omega]_i/[nl\Delta\Omega]_e$ ratio was derived from a Monte Carlo simulation of the different slits and diaphragms that defined the electrostatic analyzer and ion detector.

One must consider two opposing effects connected to the energy E of the incident projectile: the E^{-2} Rutherford dependence of the elastic scattering cross sections and the decrease of the beam current with that of its energy. We therefore used 25-keV H_3^+ projectiles, instead of protons, in order to improve the feasibility of our normalization procedure

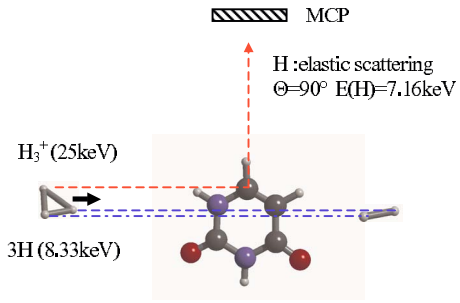

FIG. 1. (Color online) Schematic of the normalization procedure (see text). Elastic scattering, at right angle, in H_3^+ (25 keV)+uracil collisions. The scattered particles are identified by time-of-flight spectrometry and detected by a multichannel plates package.

(see Fig. 1 for the schematic). The cost to pay is one extra step. Due to the small impact parameter in the elastic scattering at right angles ($b\approx0.01$ a.u.), itself obviously smaller than the internuclear distances within the H_3^+ molecule (≈1–1.4 Å), we estimate that an H_3^+ molecule behaves like a stack of three decoupled protons [20], each of them having a kinetic energy 25/3 keV, i.e., 8.3 keV. The single differential cross sections for the elastic scattering of a proton by a uracil base were evaluated from the atomic ones using the additivity rule. This is expressed as follows: $(\partial\sigma_i/\partial\Omega_{iH_3\rightarrow molecule})=3x\Sigma_{compound k\neq H}(\partial\sigma_i/\partial\Omega_{iH\rightarrow k})$. The atomic scattering cross sections were obtained from the interaction potential of the $H^{+,0}$+C, N, O systems, i.e., the compounds of the biological target. Several descriptions were used (ZBL, Bohr, Moliere [21]), in addition to a description that made use of the electrostatic interaction between charge distributions calculated from wave functions given by the Cowan code [22]. All these descriptions gave, as they should, consistent results. Scattered protons at 90° together with 50-eV electrons that traveled within the analyzer were detected by means of a time-of-flight technique. This served discriminated electrons from spurious contributions and also identified the 7.16-keV scattered protons (165-ns time of flight in our geometry). This latter achievement required a pulsed beam. The numbers of electrons N_e and ions N_i were recorded simultaneously and mixed in the same time-of-flight spectrum using a CO4020 ORTEC multiplexing module. We estimated the uncertainty of the measured N_e/N_i ratio to be 16% and that of the calculated single differential cross sections for the elastic scattering to be about 7% (obtained by comparing different codes).

RESULTS AND DISCUSSION

The spectrum in Fig. 2(a) displays the DDCS for the production of secondary electrons at the fixed angle of $\theta=35°$ and for proton collision energies E of 25, 50 and 100 keV, in dotted, dashed, and solid lines, respectively. In contrast to our previous findings for the C_{60} molecule [12], no peaking is seen at low electron energy E_e, but instead a constant and sizeable cross-section value in the $3-6\times10^{-19}$ cm^2 eV^{-1} sr^{-1} range. Moreover, the DDCS is found to depend quite weakly upon the proton energy.

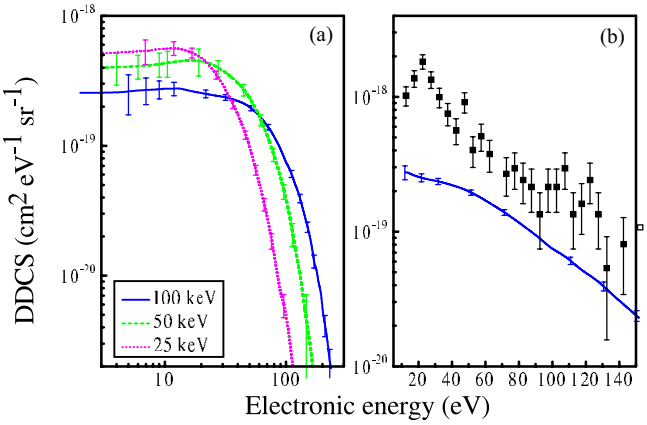

FIG. 2. (Color online) (a) Left: DDCS versus electronic energy. Three sets of data are presented for incident proton energies of 100, 50, and 25 keV, in solid, dashed, and dotted lines, respectively. (b) Right: Comparison between CTMC computation in filled squares, and experimental data in solid line.

Once we had studied the fullerene structure, a prototype of a perfect spherical system with a central potential, we interpreted the peak as the result of a barrier due to the centrifugal potential, and with the nonspherical uracil such effect should not prevail. In the high-energy part of the spectrum, according to the Bethe-Born approximation [23,24], the DDCS fall off exponentially due to the dipole interaction term that dominates. Also noticeable in this energy range is the absence of any lines originating from KLL Auger electrons of either the C, N, or O compounds (in the range 240–500 eV), whose importance was previously postulated [2,25]. This observation can be rationalized if one realizes that the total cross sections for *K*-shell ionization of C, N, and O by 100-keV proton impact are very small. These are only $1.7\ (\pm 0.1)\times 10^{-19}$, $3.6\ (\pm 0.3)\times 10^{-20}$, and $1.1\ (\pm 0.1)\times 10^{-20}$ cm^2, respectively [26].

Electron emission in ion-atom collisions has been extensively investigated and numerous models and theoretical methods are available [27]. However, such investigations for molecules, i.e., the determination of DDCS, are more difficult. One has to determine the wave functions for the initial bound state and final free states. If the former can be evaluated by molecular codes used in quantum chemistry, the evaluation of the latter wave functions is a very difficult task due to the nonspherical nature of the potential acting on a given electron in a molecule. For instance, to circumvent this nontrivial issue, Galassi *et al.* [28] used two approximations in the determination of DDCS of small molecules (CO, N_2, CH_4, CO_2) in which the multicenter features of the molecule are eliminated: Bragg's additivity rule and a molecular representation of the bound state target wave function. In the latter approximation, the cross section is decomposed as a linear combination of atomic cross sections in which the coefficients are derived from molecular calculations. Atomic DDCS are then calculated by the Continuum Distorted Wave-Eikonal Initial State (CDW-EIS) method. In their study of water ionization by electrons, Champion *et al.* [29] used a different approach: they rigorously calculated the potential acting on a given electron and then used the spherical average approximation to account for the nonorientation of the molecule. While doing this, the resulting potential had the right spherical symmetry, and subsequently, the method developed for atomic ionization could be applied (PWBA in that case). In general, good agreement was achieved with experimental data while using Galassi's and Champion's formalisms.

An alternative approach is to make use of the CTMC, and this has been successfully employed to treat ion-(di)atom collisions [30,31]. One had to describe classically the trajectory of an electron bound in a uracil molecule, the electron being perturbed by an incoming proton. The forces acting on the electron were derived from the electron-proton and electron-uracil interaction potentials evaluated with the ARGULAB 4.0.1 software [32]. The multicenter feature of the molecule was directly taken into account here. The trajectories were numerically integrated, starting from randomly chosen initial positions and velocities, but it is important to note that these did respect the binding energy of the kicked-out electron. For computational simplicity, the molecule was kept fixed in space and the proton trajectory had a random direction. In the absence of any projectile perturbation, the electron should remain bound [see Fig. 3(b)]. In order to extract the DDCS values, the initial position of the projectile was contained within an $S_{ref}=16\times 16$ a.u.^{2} surface set perpendicularly to the incident direction and centered on the uracil molecule [see Fig. 3(a)]. The cross section is then given by

$$\sigma_{(E,\theta)}=\frac{N_v N_{e(E\pm\Delta E/2,\theta\pm\Delta\theta/2)}}{N_{shot}}\frac{S_{ref}}{2\pi\sin\theta\Delta\theta\Delta E}, \qquad (4)$$

where N_v is the number of valence electrons. We first assumed that all valence electrons were equivalent (see below). The number of trajectories $N_{e(E\pm\Delta E/2,\theta\pm\Delta\theta/2)}$ represents those which lead to electron emission in the energy range $E\pm\Delta E/2$ and angle range $\theta\pm\Delta\theta/2$. N_{shot} is the total number of computed trajectories (1.8×10^6). The comparison between the experimental DDCS data, in solid line, and those from the CTMC computation, in filled squares, is presented in Fig. 2(b). Reasonable agreement is found, the calculated value overestimating the experimental data by a factor of three while assuming the equivalence of the valence electrons. In fact, the difference can be rationalized since the 42 valence electrons are indeed not equivalent. An inner shell electron is obviously more difficult to remove than an outer shell one. Taking this fact into account, we estimated, in a second step, the ionization probabilities for the 21 individual molecular orbitals (MOs) whose energies were evaluated by means of the ARGUSLAB code [32]. We calculated the ionization cross section for 100-keV incident protons, a cross section given by $\sigma_i=2\Sigma_{MO}P_{ioni}^{MO}S_{ref}$. In this expression, P_{ioni}^{MO} depicts the ionization probability of a given electron in a given MO. Including this weighting in the electron shells, we ended up with a calculated DDCS value that is lower by a factor of 1.7 compared to the case where the electron shells are treated in an equal fashion. In other words, the ratio "calculated over experimental magnitudes" has been reduced to only 1.75.

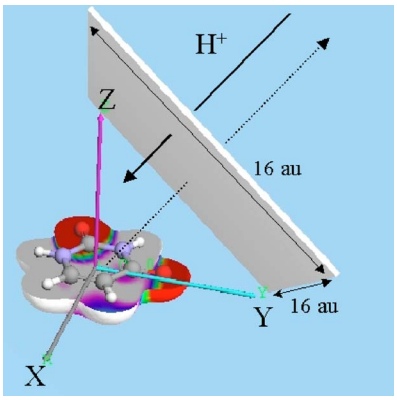

(a)

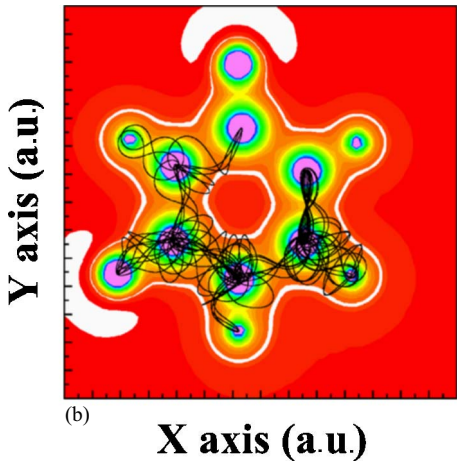

(b)

FIG. 3. (Color online) (a) Left: The uracil molecule in the *XOY* plane. The electrostatic potentials are displayed in the isodensity surface representation. The very electronegative oxygen atoms are particularly noticeable. For normalization purposes, the initial position of the projectile is contained within a 16×16 a.u.^{2} surface (see text). (b) Right: A typical trajectory.

We stress that the shapes of the calculated and experimental curves are similar, and point out that the feature at about 22 eV in the calculated curve might simply be the result of saturation in the DDCS. In the future, we plan to refine the model while generating geometries of the initial conditions closer to the molecular orbitals.

Due to their potentially large interest for track's computations, we present the single differential cross sections (SDCS) in Table I for the ejection of an electron in the solid angle ($\theta=35°$) and integrated over both 2–20 eV and 2–50 eV energy ranges. The size of these SDCSs is remarkable since they reach values as large as 1 to 2×10^{-17} cm^2 sr^{-1}.

TABLE I. the SDCS obtained by integration over the 2–20 eV and 2–50 eV ranges.

		<20 eV ($\times10^{-17}$ cm^2 sr^{-1})	<50 eV ($\times10^{-17}$ cm^2 sr^{-1})
Uracil	100 keV	0.5	1.2
	50 keV	0.8	1.8
	25 keV	1.0	1.7

CONCLUSION

This paper reports the first ever measurement of the DDCS for the emission of secondary electrons in proton-dry uracil collisions, at a fixed angle of 35°. Absolute values were extracted for the cross sections while monitoring simultaneously the elastic scattering of the projectile. No peaking was observed at low electron energy in the experimental DDCS curve but rather a constant and sizable value, the main result of the present communication. In the high energy range, we have rationalized the absence of any Auger lines. We have developed a classical trajectory Monte Carlo approach to compute the DDCS curve and we emphasize reasonable agreement with the experimental data. We plan to extend the present set of data while studying the DDCS as a function of the electron emission angles and hope this will provide new data that will be needed in biological track calculations.

ACKNOWLEDGMENTS

The authors would like to thank Alain and Daniele Bordenave-Montesquieu for their active participation in the initiation of this research program, Colin Marsden for valuable comments of the manuscript, Ali Boukabache and Pierre Cafarelli for technical support, as well as the cost P9 network.

[1] C. Le Sech, K. Takakura, C. Saint Marc *et al.*, Science **79**, 196 (2001).
[2] A. Touati, M. A. Hervé du Penhoat, B. Fayard *et al.*, Can. J. Physiol. Pharmacol. **99**, 83 (2002).
[3] B. Boudaïffa, P. Cloutier, D. Hunting *et al.*, Radiat. Prot. Dosim. **287**, 1658 (2000).
[4] F. Martin, P. D. Burrow, Z. L. Cai *et al.*, Phys. Rev. Lett. **93**, 068101 (2004).
[5] F. A. Gianturco and R. R. Lucchese, J. Chem. Phys. **120**, 7446 (2004).
[6] V. Cobut, Y. Frongillo, J. P. Patau *et al.*, Radiat. Phys. Chem. **51**, 229 (1998).
[7] T. Goulet, J. P. Patau, and J. P. Jay-Gerin, Radiat. Prot. Dosim. **31**, 33 (1990).
[8] P. Bernhardt, W. Friedland, R. Meckbach *et al.*, Radiat. Prot. Dosim. **99**, 203 (2002).
[9] L. H. Toburen, M. Dingfelder, N. Ozturk *et al.*, Radiat. Res. **161**, 106 (2004).
[10] R. Balog, M. Stano, P. Limao-Vieira *et al.*, J. Chem. Phys. **119**, 10396 (2003).

[11] P. Limao-Vieira, S. Eden, P. A. Kendall *et al.*, Int. J. Mass. Spectrom. **233**, 335 (2004).
[12] P. Moretto-Capelle, A. Rentenier, D. Bordenave-Montesquieu *et al.*, Phys. Scr., T **T110**, 325 (2004).
[13] M. E. Rudd, L. H. Toburen, and N. Stolterfoht, At. Data Nucl. Data Tables **18**, 413 (1976).
[14] H. O. Meyer, M. A. Ross, R. E. Pollock *et al.*, Phys. Rev. Lett. **65**, 2846 (1990).
[15] G. Paschmann, E. G. Shelley, C. R. Chappell *et al.*, Rev. Sci. Instrum. **41**, 1706 (1970).
[16] R. S. Gao, P. S. Gibner, J. H. Newman *et al.*, Rev. Sci. Instrum. **55**, 1756 (1984).
[17] H. O. Funsten, D. M. Suszcynsky, R. W. Harper *et al.*, Rev. Sci. Instrum. **67**, 145 (1996).
[18] S. Martin, L. Chen, A. Denis, R. Bredy, J. Bernard, and J. Desesquelles, Phys. Rev. A **62**, 022707 (2000).
[19] B. Deconihout, P. Gerard, M. Bouet *et al.*, Appl. Surf. Sci. **94/5**, 422 (1996).
[20] S. Bouneau, A. Brunelle, S. Della Negra, J. Depauw, D. Jacquet, Y. LeBeyec, M. Pautrat, M. Fallavier, J. C. Poizat, and H. H. Andersen, Phys. Rev. B **65**, 144106 (2002).
[21] W. Eckstein, *Computer Simulation of Ion-Solid Interactions*, (Springer, Berlin, 1991), p. 40.
[22] R. D. Cowan, *The Theory of Atomic Structure and Spectra* (University of California Press, 1981).
[23] H. A. Bethe, Ann. Phys. **5**, 325 (1930).
[24] M. Inokuti, Rev. Mod. Phys. **43**, 297 (1971).
[25] B. Fayard, A. Touati, F. Abel *et al.*, Radiat. Res. **157**, 128 (2002).
[26] H. Paul and J. Sacher, At. Data Nucl. Data Tables **42**, 105 (1989).
[27] N. Stolterfoht, R. D. DuBois, and R. Rivarola, *Electron Emission in Heavy Ion-Atom Collision* (Springer Series on Atoms and Plasmas, Springer 1997).
[28] M. E. Galassi, R. D. Rivarola, M. Beuve, G. H. Olivera, and P. D. Fainstein, Phys. Rev. A **62**, 022701 (2000).
[29] C. Champion, J. Hanssen, and P. A. Hervieux, Phys. Rev. A **65**, 022710 (2002).
[30] R. E. Olson, Phys. Rev. A **27**, 1871 (1983).
[31] R. E. Olson, J. Ullrich, and H. Schmidt-Böcking, Phys. Rev. A **39**, 5572 (1989).
[32] M. Thompson, Planaria Software, LLC (Seattle, WA, 2004) www.arguslab.com